JACS
JOURNAL OF THE AMERICAN CHEMICAL SOCIETY

ARTICLE

pubs.acs.org/JACS

Photocontrol over the Disorder-to-Order Transition in Thin Films of Polystyrene-*block*-poly(methyl methacrylate) Block Copolymers Containing Photodimerizable Anthracene Functionality

Wei Chen,[†,∥] Jia-Yu Wang,[‡] Wei Zhao,[†] Le Li,[†] Xinyu Wei,[†] Anna C. Balazs,[§] Krzysztof Matyjaszewski,[⊥] and Thomas P. Russell*[,†]

[†]Department of Polymer Science and Engineering, University of Massachusetts-Amherst, Amherst, Massachusetts 01003, United States

[‡]Department of Chemistry, University of Chicago, Chicago, Illinois 60637, United States

[§]Department of Chemical Engineering, University of Pittsburgh, Pittsburgh, Pennsylvania 15261, United States

[⊥]Department of Chemistry, Carnegie Mellon University, Pittsburgh, Pennsylvania 15213, United States

Supporting Information

ABSTRACT:

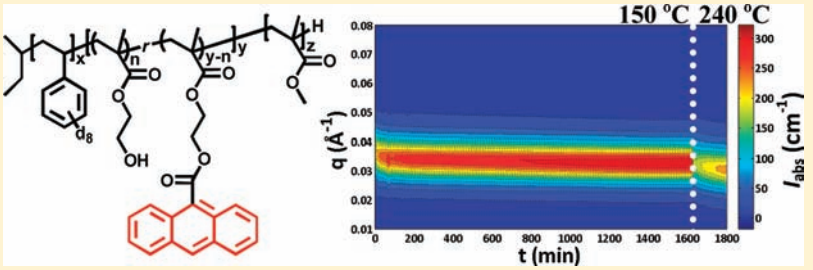

Reversible photocontrol over the ordering transition of block copolymers (BCPs) from a disordered state to an ordered state, namely the disorder-to-order transition (DOT), can be used to create long-range ordered nanostructures in self-assembled BCPs over macroscopic distances by photocombing, similar to the classic zone refining used to produce highly pure, large single crystals. Here, we have designed and synthesized an anthracene-functionalized tri-BCP containing deuterated polystyrene (d_8-PS) and poly(methyl methacrylate) (PMMA) blocks, as well as a short middle block of poly(2-hydroxyethyl methacrylates) (PHEMA) that is randomly functionalized by anthracene. This tri-BCP maintains the order-to-disorder transition-type phase behavior of its parent d_8-PS-*b*-PMMA di-BCPs. Under 365 nm UV irradiation, the junction between d_8-PS and PMMA blocks is photocoupled through the anthracene photodimers, leading to a significant increase in the total molecular weight of the tri-BCP. As a consequence, when the tri-BCP is phase-mixed but close to the boundary of the ordering transition, it undergoes the DOT, as evidenced by small-angle neutron scattering and transmission electron microscopy. The tri-BCP could be reversibly brought through the DOT in thin films by taking advantage of photodimerization and thermal dissociation of anthracene. Currently, anthracene-functionalized d_8-PS-*b*-PMMA BCP is one of the most promising candidates for the photocombing process to promote long-range laterally ordered nanostructures over macroscopic distances in a noninvasive manner.

INTRODUCTION

As one of the most effective systems for the fabrication of nanoporous thin films, polystyrene-*block*-poly(methyl methacrylate) (PS-*b*-PMMA) diblock copolymer (di-BCP), which consists of PS and PMMA polymer chains joined together at one end with a covalent bond, has been extensively studied in the past decades.[1−11] Owing to the positive mixing enthalpy and low mixing entropy of the component segments, dissimilar PS and PMMA blocks tend to phase-separate into ordered arrays of microdomains, tens of nanometers in size. Depending on the volume fraction of one block, f, and the degree of microphase separation, χN, where χ is the Flory−Huggins segmental interaction parameter (usually parametrized as $\chi = A + B/T$) and N is the number of segments in the BCP, morphologies including arrays of spherical, cylindrical, or lamellar microdomains are formed in PS-*b*-PMMA BCPs.[12] Exposure to UV radiation cross-links PS, degrades PMMA, and, by removal of the degradation products with an acetic acid rinse, produces a PS film with an array of nanopores that penetrate through the film. By etching the film, the nanopattern of the BCP template can be transferred to the underlying substrate, like metals, semiconductors, and plastics. This templating process, developed by Hawker and Russell,[2−6] has been used in a flash memory application by Black and Guarini.[13−17] Most recently,

Received: April 21, 2011
Published: September 11, 2011

IBM has also fabricated air-gap insulators derived from the self-assembly of PS-*b*-PMMA di-BCPs, claimed as "the first-ever application of a breakthrough self-assembling nanotechnology to conventional chip manufacturing".[18,19] At present, PS-*b*-PMMA is considered as an exceptionally promising system for generating nanostructured templates and scaffolds with controllable feature sizes down to ~12 nm. However, for applications requiring addressability, the challenge remains to achieve a long-range order of PS and PMMA microdomains over macroscopic length scales, due to the weak segmental interactions between the PS and PMMA and the formation of defects like grain boundaries, edge dislocations, and disclinations. Consequently, external fields are needed to remove the defects and enhance the order of the microdomains.

Recently, Balazs and co-workers[20,21] proposed that defect-free structures in thin films over macroscopic distances could be produced by reversibly bringing polymer blends through a morphological transition from a homogeneous mixture to a phase-separated state using a photocombing process. In this process, the polymer blend film is swept by bands of light with different wavelengths, forcing phase mixing and then phase separation, where the phase separation is templated by the exiting phase-separated mixture. This hypothesis is based on experimental studies[22−26] in which phase separation in a binary polymer blend of *trans*-stilbene-labeled PS and poly(vinyl methyl ether) (PSS/PVME) was reversibly induced by photochemical reactions. Meanwhile, Hashimoto and co-workers[27−33] also produced highly ordered BCP microdomains by slowly moving a temperature gradient, instead of light, across the BCP film to induce the disorder-to-order transition (DOT). In this case, when the BCP ordered, the BCP microdomains were epitaxially "crystallized" in a moving front, creating macroscopically ordered nanostructures—a single-grain lamellar structure[27,28] and a columnar grain texture having a special orientation of hexagonally packed cylindrical microdomain structure.[29−33] In addition, directionally selective light excitation has been employed to fabricate patterned and oriented BCP microdomains in liquid-crystal and other relevant systems.[34−37] For instance, Seki and co-workers reported an optical 3-D alignment of cylindrical microdomains of a BCP comprising photoresponsive liquid-crystal block chains and poly(ethylene oxide) (PEO) through the process of photoinduced mass migration.[36] Ikeda and co-workers used a polarized laser to control parallel patterning of PEO nanocylinders in an amphiphilic, liquid-crystalline BCP film.[37]

It is well-known that anthracene, a solid polycyclic aromatic hydrocarbon consisting of three fused benzene rings, has the ability to photodimerize by UV irradiation via a [4π+4π] cycloaddition.[38] The resulting photodimers can also be reversed either thermally at an elevated temperature higher than 180 °C or with UV irradiation with the wavelength below 300 nm. Tran-Cong-Miyata and co-workers have utilized anthracene photodimerization to tune the phase transition in a polymer blend of an anthracene-labeled PS (PSA) and poly(vinyl methyl ether) (PVME).[26,39,40] Upon irradiation with 365 nm UV light, anthracene moieties undergo photodimerization, leading to phase separation of the two polymers, whereas by exposure to 297 nm UV light, the photodimers are converted back to anthracene monomers, homogenizing the phase-separated blend. In addition, the resulting bicontinuous structure in the polymer blend on various length scales was controlled by periodic irradiation.[26] Thus, by combining the advances associated with PS-*b*-PMMA BCPs and the high efficiency of photodimerizable anthracene, as shown in the case of the PSA/PVME blend, the long-range laterally ordered nanostructures of PS-*b*-PMMA could be created over macroscopic scales through the photocombing of anthracene-functionalized PS-*b*-PMMA BCPs by taking advantage of the photocontrollable DOT.

Scheme 1. Synthetic Pathway of d_8-PS-*b*-P(9AnEMA-*r*-HEMA)-*b*-PMMA BCPs

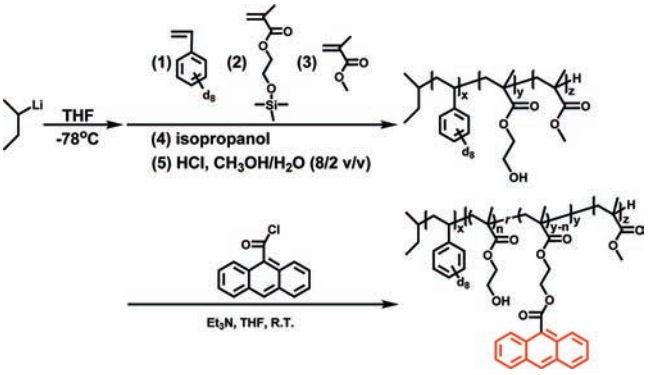

The key to achieve photocombing is the reversible photocontrol over the DOT in anthracene-functionalized PS-*b*-PMMA BCP films. In this work, we show the photocontrol over the DOT of a triblock copolymer (tri-BCP), deuterated polystyrene-*block*-poly(2-hydroxyethyl methacrylate-*random*-2-(methacryloyloxy)-ethyl anthracene-9-carboxylate)-*block*-poly(methyl methacrylate) (d_8-PS-*b*-P(9AnEMA-*r*-HEMA)-*b*-PMMA), in which the short middle block of poly(2-hydroxyethyl methacrylates) (PHEMA) is partially functionalized by anthracene in a random manner. The tri-BCP, with a molecular weight (MW) of M_n = 26 000 (designated as Tri26k), exhibits an order-to-disorder transition (ODT) upon heating, similar to the parent PS-*b*-PMMA di-BCP with M_n = 28 000 (designated as Di28k). Upon UV irradiation, the photodimerization of anthracene resulted in a significant increase in the total MW of the copolymer. Consequently, the DOT was induced in a thin film, as evidenced by small-angle neutron scattering (SANS) and transmission electron microscopy (TEM). In addition, *in situ* SANS measurements confirmed that this tri-BCP could be reversibly brought through the DOT in films by the photodimerization and thermal dissociation of anthracene.

RESULTS AND DISCUSSION

Phase Behavior. The phase behavior of PS-*b*-PMMA di-BCP has been studied using various scattering techniques. The copolymer exhibited an ODT upon heating, and its χ possesses a strong entropic contribution and a relatively weak enthalpic contribution. For a symmetric PS-*b*-PMMA di-BCP with a MW of ~28 000, the ODT locates within an experimentally accessible temperature range.[41−47] For the studies on the reversible photocontrol over the DOT, the Tri26k BCP was synthesized by a sequential anionic polymerization with a postfunctionalization (Scheme 1). The molecular characteristics and composition are given in Table 1. On average, the partially anthracene-functionalized HEMA middle block contains five repeat units, in which three anthracene functional groups were randomly incorporated. Even though Tri26k BCP is called a tri-BCP following the tradition, it is effectively a di-BCP with a large junction.

As is well-known, the ODT can be determined from scattering measurements. Using mean-field theory, Leibler theoretically

Table 1. Characteristics of d_8-PS-*b*-PMMA Di-BCP and d_8-PS-*b*-P(9AnEMA-*r*-HEMA)-*b*-PMMA Tri-BCP[a]

	M_n	M_w	PDI	$f_{d_8\text{-PS}}$
Tri26k	26 000	28 000	1.07	46%
Di28k	28 000	30 000	1.06	53%

[a] The weight fraction of d_8-PS, P9AnEMA, PHEMA, and PMMA for the Tri26k BCP was determined by GPC and ^{1}H NMR as 45.5:3.3:0.9:50.3 (%).

described the behavior of di-BCPs undergoing an ordering transition.[48] The theory predicts that the scattered intensity $I(q)$ in the disorder state is given by

$$[I(q)/N]^{-1} \approx F(q) - 2\chi N \quad (1)$$

where q is the scattering wave vector ($q = 4\pi \sin\theta/\lambda$, λ is the wavelength, and 2θ is the scattering angle) and $F(q)$ is a function which depends on the radius of gyration R_g and the composition f. $F(q)$ has a minimum, and, consequently, $I(q)$ has a maximum intensity I_{max} at q^*. The inverse maximum intensity, I_{max}^{-1}, in the disordered state depends linearly on the inverse temperature, T^{-1}, and is zero at the spinodal temperature, T_S, of the ODT, provided that χ is inversely proportional to temperature, i.e., $\chi = A + B/T$. A deviation of I_{max}^{-1} from linearity occurs due to density fluctuations in the vicinity of the ODT,[47] and hence T_{ODT} is lower than T_S. Consequently, the ODT is a fluctuation-induced first-order phase transition.

The intensity of scattering $I(q)$ in eq 1 can be rewritten as[49,50]

$$I(q) \sim \frac{I_{max}}{1 + 4(q - q^*)^2(\Delta q)^{-2}} \quad (2)$$

where Δq represents the full width at half-maximum (fwhm) of the peak. So,

$$\Delta q^2 = \frac{1}{\xi^2} \sim \left(\frac{1}{R_g^2}\right)\left(\frac{\chi_S - \chi}{\chi_S}\right) \sim \frac{1}{N}\left(\frac{\chi_S - \chi}{\chi_S}\right) \sim \frac{1}{T_S} - \frac{1}{T} \quad (3)$$

and

$$\left(\frac{I_{max}}{N}\right)^{-1} \equiv \left(\frac{I(q^*)}{N}\right)^{-1} \approx F(q^*) - 2\chi N$$
$$= 2(\chi_S - \chi)\, N \sim \left(\frac{1}{T_S} - \frac{1}{T}\right)N \quad (4)$$

where χ_S is the χ value at T_S. So, Δq^2 is very sensitive to the ODT. In the following discussions, we follow the definition of the DOT and use the term "ordering" to describe the phase transition of the block copolymer from a homogeneous, disordered state to a phase-separated, ordered state without further notice.

Figure 1 shows the temperature-dependent SANS profiles of both Tri26k and Di28k BCPs. The absolute scattering intensity, $I_{abs}(q)$, is plotted as a function of the magnitude of scattering vector q. Continuous changes in peak intensity and width are seen for both the Tri26k and Di28k BCPs. As temperature increases, the maximum weakens and broadens, in keeping with the correlation-hole scattering of a disordered BCP melt. In Figure 2, I_{max}^{-1} and Δq^2 for both Tri26k and Di28k are shown as functions of T^{-1}. Both I_{max}^{-1} and Δq^2 vary linearly with T^{-1} at temperatures higher than T_{MF}, ~160 °C for Tri26k BCP and ~210 °C for Di28k BCP, respectively, in agreement with the mean-field arguments. Linearly extrapolating I_{max}^{-1} (Δq^2) vs T^{-1} to $I_{max}^{-1} = 0$, T_S was found to be ~135 °C for Tri26k BCP and ~160 °C for Di28k BCP, respectively. Below T_{MF}, I_{max}^{-1} and Δq^2

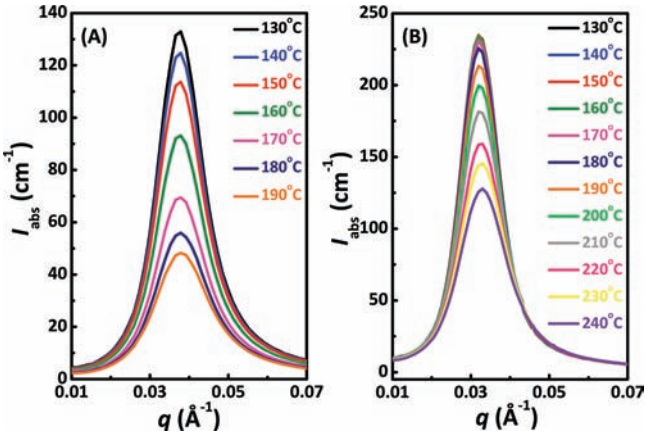

Figure 1. Temperature dependence of the SANS profiles near the primary scattering maxima for (A) Tri26k in the range from 130 to 190 °C and (B) Di28k in the range from 130 to 240 °C with an interval of 10 °C.

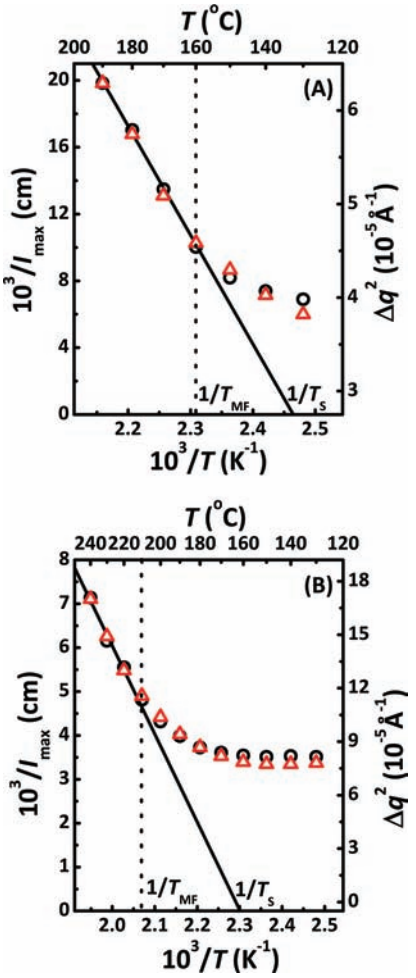

Figure 2. I_{max}^{-1} (black circles) and Δq^2 (red triangles) plotted as a function of the inverse temperature for (A) Tri26k and (B) Di28k BCPs.

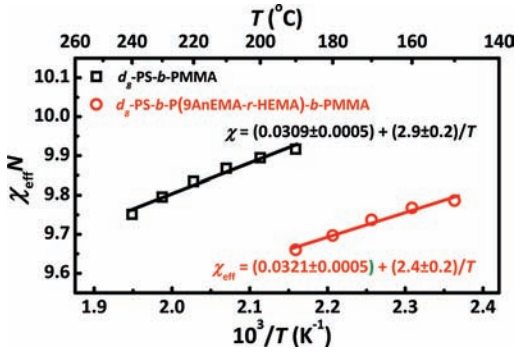

Figure 3. Temperature dependence of $\chi_{eff}N$ estimated from SANS data for Tri26k (red circles) and Di28k (black squares) using a smeared RPA fitting.

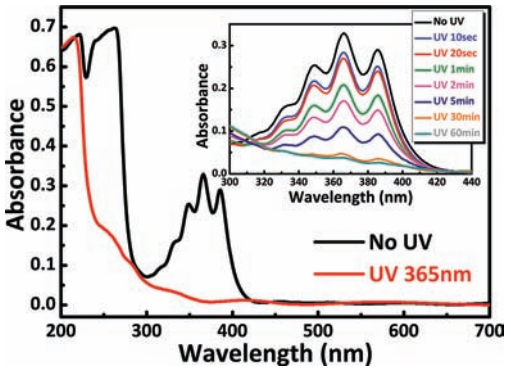

Figure 4. Representative UV−vis absorption spectra of a Tri26k film with a thickness of ~1 μm on a UV-transmitted quartz slide as a function of the exposure time to UV light with a wavelength of 365 nm and an intensity of 35 mW/cm^2 at 150 °C. The film was pre-annealed at 150 °C under vacuum for 48 h.

deviate from linearity due to composition fluctuations. Since no sharp discontinuities of I_{max}^{-1} and Δq^2 for both Tri26k and Di28k were observed, T_{ODT} could not be clearly discerned, as it is below either the measured temperature range or the glass transition temperature of the BCPs. Up to this point, it is evident that the Tri26k BCP exhibits an ODT-type phase behavior, similar to the Di28k BCP. Both Tri26k and Di28k are in the disordered state, but very close to the boundary of ordering transition from the disordered state.

The effective χ can be estimated from the structure factor, $S(q)$, modified for the effects of polydispersity and asymmetry in the segmental volume, in the disordered state by

$$\frac{N}{S(q)} = F(q) - 2\chi_{eff}N \tag{5}$$

where $F(q)$ is a combination of correlation functions for an unperturbed (Gaussian) di-BCP, N is the overall degree of polymerization, and χ_{eff} is the effective interaction parameter. An equivalent form which includes the effect of polydispersity was given by Benoit and co-workers[51] as

$$F(q) = \frac{x_1 + x_2 + 2x_{12}}{x_1x_2 - x_{12}^2} \tag{6}$$

Based on a Zimm−Schultz distribution,[52,53]

$$x_i = 2f_i\left[\frac{1}{z_i} - \frac{1}{z_i^2} + \frac{1}{z_i^2}\left(\frac{1}{1 + [z_i/(k_i - 1)]}\right)^{k_i - 1}\right] \tag{7}$$

where

$$k_i = \left(1 - \frac{1}{M_w/M_n}\right)^{-1} \tag{8}$$

and

$$z_i = \frac{q^2a_i^2N_i}{6} \tag{9}$$

where a_i is the statistical segment length.

The SANS profiles calculated for Tri26k and Di28k BCPs are indicated by solid lines in Supporting Information Figures S2 and S3, respectively, and the corresponding $\chi_{eff}N$ values at each temperature are shown in Figure 3. The agreement between the calculations and the experimental data is reasonable over the entire scattering vector range. $\chi_{eff}N$ values are in the range of ~9.6−10, which is close to the critical value of $(\chi N)_{ODT}$ = 10.495 for a symmetric di-BCP, quantitatively confirming that Tri26k and Di28k are phase-mixed but very close to the boundary of the ODT. In addition, the random phase approximation (RPA) of tri-BCPs[54] was applied to fit the SANS profiles of Tri26k BCP, but it cannot describe our experimental data as well as that of di-BCPs, and the parameters obtained from the best fit, such as segmental lengths and interaction parameters, are not reasonable either. These results support our treatment of Tri26k BCP as a di-BCP in the RPA theory.

The linear least-squares fits to the resultant χ values as a function of T^{-1} yield $\chi_{eff} = (0.0321 \pm 0.0005) + (2.4 \pm 0.2)/T$ for the d_8-PS-b-P(9AnEMA-r-HEMA)-b-PMMA BCP and $\chi = (0.0309 \pm 0.0005) + (2.9 \pm 0.2)/T$ for the d_8-PS-b-PMMA BCP. The χ values for the d_8-PS-b-PMMA BCP are consistent with the literature: $\chi = 0.0282 + 3.9/T$ for a d_8-PS-b-PMMA BCP with M_n = 27 700 and $f_{d_8\text{-PS}} = 0.44$;[41,55] $\chi = 0.0292 + 3.2/T$ for a PS-b-d_8-PMMA BCP with M_n = 27 000 and $f_{PS} = 0.05$;[55] $\chi = 0.0251 + 3.2/T$ for a d_8-PS-b-d_8-PMMA BCP with M_n = 32 600 and $f_{d_8\text{-PS}} = 0.48$;[55] $\chi = 0.0294 + 3.2/T$ for a d_8-PS-b-PMMA BCP with M_n = 28 000 and $f_{d_8\text{-PS}} = 0.53$;[42] $\chi = 0.0282 + 4.46/T$ for a PS-b-PMMA BCP with M_n = 25 700 and $f_{PS} = 0.53$;[46] $\chi = 0.021 + 3.2/T$ for homopolymer blends of PS and PMMA, determined from cloud point measurements.[56]

UV-Induced DOT. Since photodimerization depends on the anthracene mobility in the anthracene-containing compound,[57,58] the efficiency of anthracene photodimerization was investigated by time-dependent UV−vis absorption spectra. As shown in Figure 4, the typical [4π+4π] anthracene cyclodimerization reactions were monitored by time-dependent UV−vis absorption spectroscopy on a thin film of Tri26k BCP (spin-coated on quartz plate, thickness ~1 μm) in a N_2 gas environment illuminated with a high-pressure mercury lamp (λ = 365 nm, I_{UV} = 35 mW/cm^2). Anthracene absorption bands[59] both between 350 and 410 nm and at 265 nm gradually decrease with increasing exposure time, nearly disappearing after 1 h of irradiation. Obviously, the photodimerization of anthracene in the films of Tri26k BCP is highly efficient, and almost all the anthracene functional groups are transformed into photodimers after exposure to 365 nm UV light for 1 h.

SANS profiles in Figure 5 show the influence of anthracene photodimerization on the phase behavior of Tri28k BCP in films. After 1 h of UV irradiation at 150 °C, the absolute intensity of the

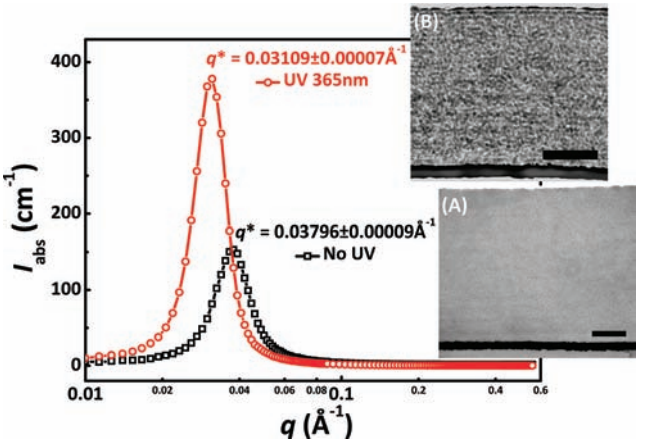

Figure 5. SANS profiles of Tri26k films before (black) and after (red) exposure to UV light with a wavelength of 365 nm and an intensity of 35 mW/cm^2 for 1 h at 150 °C in N_2. The films were pre-annealed at 150 °C under vacuum for 48 h. Insets: The corresponding cross-sectional TEM images of the films of Tri26k BCP before (A) and after (B) UV irradiation (scale bar = 100 nm).

scattering, I_{max}, increases more than 2-fold and the position of scattering peak, q^*, shifts from 0.03796 Å to a much lower value of 0.03109 Å, indicating that the UV-induced ordering transition from a disordered to an ordered state occurred in the copolymer film. TEM images further support the UV-induced DOT and demonstrate this transformation more directly. Figure 5A is a typical TEM image of a homogeneous, phase-mixed BCP, while the TEM image in Figure 5B captures a kinetically trapped state in the copolymer film after UV irradiation and shows worm-like and random-oriented lamellar microdomains with a period of ~20 nm, in agreement with the SANS results. Upon UV irradiation, the photodimerization of anthracene functionalities leads to a significant increase in the total MW of Tri26k BCP, thereby inducing the DOT in the thin film of phase-mixed Tri26k BCP, as indicated by the slower dissolution of the UV-irradiated films than those films without UV irradiation. Regarding the photochemistry involved,[38,57] the photocoupling at the junction between d_8-PS and PMMA blocks leads to an increase in the total molecular weight and the formation of H-type or even more branching macromolecular architectures, both of which would significantly increase the physical entanglement among BCP chains and, thereby, make the BCP more difficult to dissolve.

Reversibility. The UV-induced DOT in the thin film of phase-mixed Tri26k BCP was further investigated by *in situ* SANS. Initially, the Tri26k BCP film was exposed to UV light at room temperature, well below the T_g of the blocks of Tri26k BCP. Thus, the copolymer chains were frozen in the film, even though the anthracene functional groups were converted into photodimers. Once the film was heated to 150 °C, which is above the T_g of the blocks, a DOT was observed. Consequently, the UV-induced DOT could be monitored by changes in the SANS profiles (Figure 6A). Since the photodimerization of anthracene is thermally reversible, the BCP was driven through the ODT by heating the Tri26k BCP film to 240 °C, as shown in the SANS data in Figure 6. Reversible control over the DOT in the Tri26k BCP film was quantitatively evidenced by the time-dependence of the absolute intensity of the scattering maximum, I_{max} (Figure 6B), and the squared fwhm of the peak, Δq^2 (Figure 6C). I_{max} and Δq^2 have the same trend as the contour maps. After heating to 240 °C,

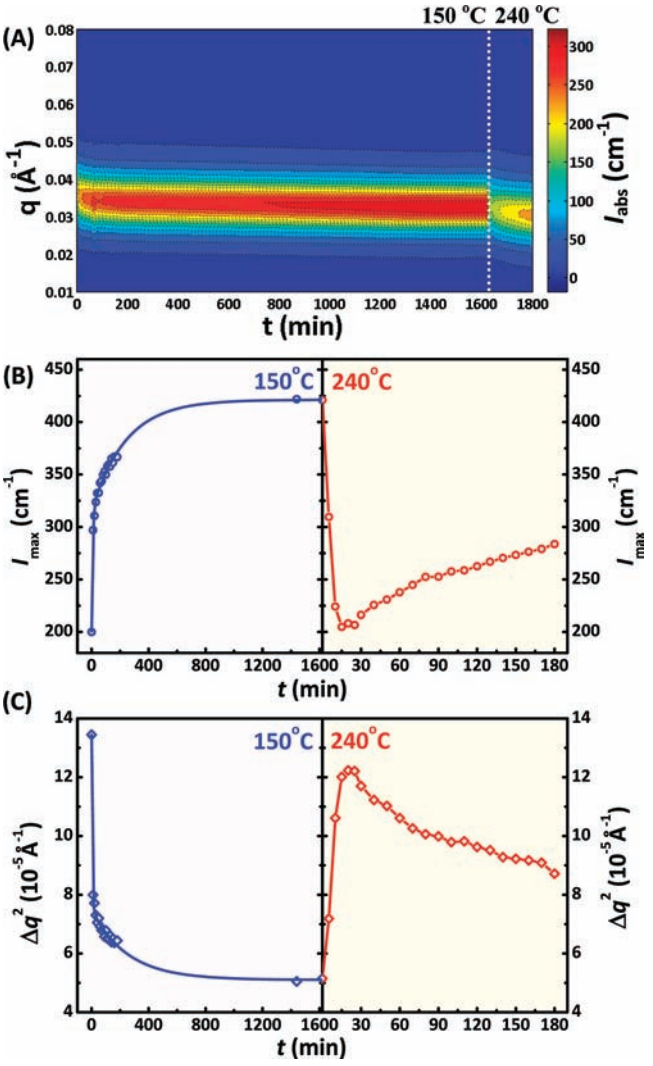

Figure 6. (A) Contour map of the absolute scattering intensity obtained from *in situ* SANS measurements as functions of the annealing time t and wave vector q. The color bar on the right illustrates the scale of the absolute scattering intensity. After exposure to UV light with a wavelength of 365 nm and an intensity of 35 mW/cm^2 for 1 h, the Tri26k BCP film was heated to 150 °C and annealed for 27 h, monitored by *in situ* SANS measurements, followed by 3 h annealing at 240 °C. The white dotted line indicates that the temperature increases from 150 to 240 °C. (B,C) Corresponding time dependence of the absolute intensity of the primary scattering maximum I_{max} (B) and the squared fwhm of the peak Δq^2 (C), both of which are obtained from the smeared Lorentzian fits of *in situ* SANS profiles for the Tri26k BCP film according to eq 2.

both I_{max} and Δq^2 nearly revert to the original values. It should be noted that, after the thermo-induced ODT, I_{max} increases and Δq^2 decreases, indicating that the tri26k BCP film tends to order again. This more than likely arises from the incomplete thermal dissociation of the anthracene or the side reactions upon annealing the film at the high temperature (240 °C). Initially, the system is kinetically trapped in the disordered state. With increasing the annealing time at elevated temperatures, the side reactions, due to the formation of radicals in the process of anthracene dissociation,[58] are even more severe. Any remnant of the photocoupled copolymer chains would tend to drive the system back toward the ordered state. From the representative

UV−vis spectra of Tri26k BCP film (Supporting Information Figure S4), less than 40% of the anthracene rings re-formed after the thermal dissociation, as evidenced by the reappearance of the anthracene absorption bands between 350 and 410 nm and at 265 nm. Therefore, in light of the recent work by Tran-Cong-Miyata and co-workers,[40] the photodissociation of anthracene with 297 nm UV light is highly desired to enhance the reversibility of UV-induced DOT in the d_8-PS-*b*-P(9AnEMA-*r*-HEMA)-*b*-PMMA tri-BCP, since the efficiency and reaction rate of anthracene photodissociation are much higher than those of the thermal dissociation. These technical issues, however, do not alter our conclusions on the reversible photocontrol over the DOT in the d_8-PS-*b*-P(9AnEMA-*r*-HEMA)-*b*-PMMA tri-BCP.

EXPERIMENTAL SECTION

Synthesis of d_8-PS-*b*-PMMA and d_8-PS-*b*-P(9AnEMA-*r*-HEMA)-*b*-PMMA. The d_8-PS-*b*-PMMA di-BCP used in this study was synthesized by the sequential anionic polymerization of styrene (St) and methyl methacrylate (MMA) in tetrahydrofuran (THF) at −78 °C under a purified argon environment using *sec*-butyllithium as an initiator. The d_8-PS-*b*-P(9AnEMA-*r*-HEMA)-*b*-PMMA tri-BCP composed of PS and PMMA, as well as a short middle block of partially anthracene-functionalized 2-hydroxyethyl methacrylates (HEMA), was obtained through the combination of sequential anionic polymerization and an esterification reaction for anthracene postfunctionalization (Scheme 1), similar to the preparation of d_8-PS-*b*-P(*n*BMA-*r*-AzoEMA) BCPs reported previously.[60,61] Table 1 gives the characteristics of Di28k and Tri26k BCPs. MWs and PDIs of Di28k and Tri26k BCPs were characterized by gel permeation chromatography (GPC), and their compositions were determined by ^{1}H NMR spectroscopy.

Characterization. NMR spectra were recorded in $CDCl_3$ on a Brüker Avance 400 (^{1}H) spectrometer with a Brüker BBO5 probe. A Knauer K-501 Pump with a K-2301 refractive index (RI) detector and K-2600 UV detector, as well as a column bank consisting of two Polymer Laboratories PLGel Mixed D columns and one PLGel 50 Å column (15 × 300 mm) in THF as eluent at a flow rate of 1.0 mL/min against linear PS standards, was used for GPC measurements. UV−vis absorption spectra were recorded on a Perkin-Elmer Lambda 850 UV−vis spectrophotometer. Film thickness was measured with a Rudolph Research AutoEL-II ellipsometer using a helium−neon laser (λ = 632.8 nm) at a 70° incidence angle and a Filmetrics F20-UV thin-film measurement system (Filmetrics Inc.) with a regulated deuterium and tungsten−halogen high-power UV−vis fiber light source (Hamamatsu Inc.) over a wavelength range from 200 to 1100 nm with the incident light normal to the sample surface. TEM experiments were performed on a JEOL TEM200CX instrument at an accelerating voltage of 200 kV. To prepare TEM samples, a thin layer of gold (~20 nm) was first evaporated onto the surface of copolymer films. Subsequently, the copolymer films with the thin gold layer were embedded into epoxy and then cured at 60 °C overnight. After the samples were dipped into liquid nitrogen, the films were transferred from the substrate to the surface of the epoxy. All the samples were microtomed at room temperature with a diamond knife into 30−50 nm thickness sections and then collected on copper grids. Before TEM observations, the thin sections were exposed to ruthenium tetraoxide vapor for ~25 min to enhance the contrast.

Small-Angle Neutron Scattering (SANS). SANS measurements were performed at the Cold Neutron Research Facility at the National Institute of Standards and Technology (NIST) on the NG3 and NG7 30m SANS instruments. For NG3 SANS, the wavelength of the neutron beam was λ = 6 Å, with $\Delta\lambda/\lambda$ = 0.15. Each measurement was performed in two different instrument configurations: one with the detector offset by 20 cm and a sample-to-detector distance (SDD) of 205 cm, and the other with a SDD of 505 cm, resulting in a q range of 0.007−0.3 Å^{-1}. For NG7 SANS, the wavelength of neutrons was λ = 6 Å, with $\Delta\lambda/\lambda$ = 0.11. Two configurations were used: one with the detector offset by 20 cm and a SDD of 105 cm, and the other with a SDD of 405 cm, giving a q range of 0.008−0.5 Å^{-1}. Some measurements were also taken on CG2 SANS at the High Flux Isotope Reactor (HFIR), Oak Ridge National Laboratory, with a different instrument configuration, characterized by a nominal SDD of 10 817 cm, leading to a q range of 0.005−0.12 Å^{-1}. For CG2 SANS, neutrons of wavelength λ = 4.8 Å, with $\Delta\lambda/\lambda$ = 0.12, were used. The scattered intensity was corrected for instrument dark current, empty cell scattering, the sensitivity of individual detector pixels, and beam transmission to obtain the absolute neutron intensity by using the available data reduction macros based on the Igor Pro data analysis package through the direct beam flux method.[62] Data were analyzed by the smeared incompressible RPA model by Leibler, Fredrickson, Helfand, and co-workers.[12,48,63−70] The program codes for smeared incompressible RPA analysis were modified from the Igor procedure in the SANS data analysis package provided by NCNR, NIST. The incoherent scattering was set as one of the fitting parameters and was corrected for the fitting results.

Bulk samples for the SANS measurements were prepared by compression-molding the annealed Di28k and Tri26k BCPs into 1.5 cm diameter disks with a thickness of ~500−800 μm at 130 °C. The disks were then annealed at 130 °C under vacuum for 72 h. Samples for analysis were placed into demountable titanium cells fitted with quartz windows. The entire assembly was mounted on a remote-controlled multisampling block with a heating setup designed for the neutron spectrometer. Prior to each measurement, the samples were allowed 30 min to achieve thermal equilibrium. The temperature was monitored and controlled by a thermocouple located in close proximity to the samples. The temperature control was within ±1 °C at each temperature. To investigate the effects of UV irradiation, the Newport-Oriel light source equipped with a high-power mercury arc lamp (500 W), a digital light intensity controller, and a 365 nm wavelength filter was used for UV light irradiation. Since most chemical reactions promote inhomogeneously in the bulk state of polymers, UV-induced DOT experiments were performed on films with thicknesses of ~800 nm spin-coated from a toluene solution of Tri26k BCP onto Si wafers. All the films were handled under two different environments after pre-annealing at 150 °C under vacuum for 48 h. One keeps the films in the dark, and the other exposes the films to 365 nm UV light with an intensity of 35 mW/cm^2 for 1 h at 150 °C under N_2. In addition, *in situ* SANS was performed to monitor the kinetics of ordering transitions associated with the photodimerization and thermal dissociation of anthracene, that is, UV-induced DOT and thermal homogenization in the Tri26k BCP film.

CONCLUSIONS

Partially anthracene-functionalized PHEMA as a middle block was successfully incorporated into a d_8-PS-*b*-PMMA, forming a d_8-PS-*b*-P(9AnEMA-*r*-HEMA)-*b*-PMMA tri-BCP. This tri-BCP maintains an ODT-type phase behavior, similar to its parent d_8-PS-*b*-PMMA di-BCP. Upon UV irradiation, the anthracene photodimers were coupled, which significantly increased the total MW of the tri-BCP and, thereby, drove the tri-BCP through an ordering transition. In addition, reversible photocontrol over the DOT was achieved by taking advantage of photodimerization and thermal dissociation of anthracene. Our study therefore demonstrates that the long-range laterally ordered nanostructures of PS-*b*-PMMA could be created over macroscopic scales through the photocombing of anthracene-functionalized PS-*b*-PMMA BCP. Future work will be to unravel the technical aspects that hinder realizing the long-range order structure through photocombing.

■ ASSOCIATED CONTENT

Supporting Information. Temperature-dependent SANS profiles and their corresponding smeared RPA calculations. This material is available free of charge via the Internet at http://pubs.acs.org.

■ AUTHOR INFORMATION

Corresponding Author
russell@mail.pse.umass.edu

Present Addresses
[||]Center for Nanoscale Materials, Argonne National Laboratory, Argonne, IL 60439

■ ACKNOWLEDGMENT

This research was supported by the Department of Energy, Office of Basic Energy Science (DE-FG02-02ER45998) and the National Science Foundation-supported Material Research Science and Engineering Center (MRSEC) at the University of Massachusetts, Amherst (DMR-0213695). We thank Dr. Y. Liu and Dr. S. Kline for the assistance with SANS measurements and Dr. B. Hammouda for helpful discussions. This work utilized facilities supported in part by the National Science Foundation under Agreement No. DMR-0454672. We acknowledge the support of the National Institute of Standards and Technology, U.S. Department of Commerce, in providing the neutron research facilities used in this work. We also thank Dr. Y. B. Melnichenko for the assistance with SANS measurements. This research at Oak Ridge National Laboratory's High Flux Isotope Reactor was sponsored by the Scientific User Facilities Division, Office of Basic Energy Sciences, U.S. Department of Energy.

■ REFERENCES

(1) Rogers, J. A.; Lee, H. H. *Unconventional Nanopatterning Techniques and Applications*; John Wiley & Sons, Inc: Hoboken, NJ, 2009.
(2) Hawker, C. J.; Russell, T. P. *MRS Bull.* **2005**, *30*, 952–966.
(3) Bang, J.; Jeong, U.; Ryu, D. Y.; Russell, T. P.; Hawker, C. J. *Adv. Mater.* **2009**, *21*, 4769–4792.
(4) Mansky, P.; Liu, Y.; Huang, E.; Russell, T. P.; Hawker, C. *Science* **1997**, *275*, 1458–1460.
(5) Thurn-Albrecht, T.; Schotter, J.; Kastle, G. A.; Emley, N.; Shibauchi, T.; Krusin-Elbaum, L.; Guarini, K.; Black, C. T.; Tuominen, M. T.; Russell, T. P. *Science* **2000**, *290*, 2126–2129.
(6) Ryu, D. Y.; Shin, K.; Drockenmuller, E.; Hawker, C. J.; Russell, T. P. *Science* **2005**, *308*, 236–239.
(7) Xu, T.; Kim, H.-C.; DeRouchey, J.; Seney, C.; Levesque, C.; Martin, P.; Stafford, C. M.; Russell, T. P. *Polymer* **2001**, *42*, 9091–9095.
(8) Xu, T.; Stevens, J.; Villa, J. A.; Goldbach, J. T.; Guarini, K. W.; Black, C. T.; Hawker, C. J.; Russell, T. P. *Adv. Funct. Mater.* **2003**, *13*, 698–702.
(9) Kim, S. O.; Solak, H. H.; Stoykovich, M. P.; Ferrier, N. J.; de Pablo, J. J.; Nealey, P. F. *Nature* **2003**, *424*, 411–414.
(10) Stoykovich, M. P.; Mueller, M.; Kim, S. O.; Solak, H. H.; Edwards, E. W.; de Pablo, J. J.; Nealey, P. F. *Science* **2005**, *308*, 1442–1446.
(11) Ruiz, R.; Kang, H.; Detcheverry, F. A.; Dobisz, E.; Kercher, D. S.; Albrecht, T. R.; de Pablo, J. J.; Nealey, P. F. *Science* **2008**, *321*, 936–939.
(12) Hamley, I. W. *The Physics of Block Copolymers*; Oxford University Press: New York, 1998.
(13) Black, C. T.; Guarini, K. W. Nonvolatile Memory Device Using Semiconductor Nanocrystals and Method Forming Same. U.S. Patent 20090311851, Dec 17, 2009.
(14) Guarini, K. W.; Black, C. T.; Yeung, S. H. I. *Adv. Mater.* **2002**, *14*, 1290–1294.
(15) Black, C. T.; Guarini, K. W.; Milkove, K. R.; Baker, S. M.; Russell, T. P.; Tuominen, M. T. *Appl. Phys. Lett.* **2001**, *79*, 409–411.
(16) Guarini, K. W.; Black, C. T.; Milkove, K. R.; Sandstrom, R. L. *J. Vac. Sci. Technol. B* **2001**, *19*, 2784–2788.
(17) Guarini, K. W.; Black, C. T.; Zhang, Y.; Kim, H.; Sikorski, E. M.; Babich, I. V. *J. Vac. Sci. Technol. B* **2002**, *20*, 2788–2792.
(18) http://www-03.ibm.com/press/us/en/pressrelease/21473.wss.
(19) *Am. Ceram. Soc. Bull.* **2007**, *86*, 8.
(20) Travasso, R. D. M.; Kuksenok, O.; Balazs, A. C. *Langmuir* **2005**, *21*, 10912–10915.
(21) Travasso, R. D. M.; Kuksenok, O.; Balazs, A. C. *Langmuir* **2006**, *22*, 2620–2628.
(22) Van-Pham, D.-T.; Trinh, X.-A.; Nakanishi, H.; Tran-Cong-Miyata, Q. *Adv. Nat. Sci.: Nanosci. Nanotechnol.* **2010**, *1*, 013002 and references therein.
(23) Tran-Cong, Q.; Kawai, J.; Endoh, K. *Chaos* **1999**, *9*, 298–307.
(24) Nishioka, H.; Kida, K.; Yano, O.; Tran-Cong, Q. *Macromolecules* **2000**, *33*, 4301–4303.
(25) Nakanishi, H.; Satoh, M.; Norisuye, T.; Tran-Cong-Miyata, Q. *Macromolecules* **2004**, *37*, 8495–8498.
(26) Tran-Cong-Miyata, Q.; Nishigami, S.; Ito, T.; Komatsu, S.; Norisuye, T. *Nat. Mater.* **2004**, *3*, 448–451.
(27) Hashimoto, T.; Bodycomb, J.; Funaki, Y.; Kimishima, K. *Macromolecules* **1999**, *32*, 952–954.
(28) Bodycomb, J.; Funaki, Y.; Kimishima, K.; Hashimoto, T. *Macromolecules* **1999**, *32*, 2075–2077.
(29) Mita, K.; Tanaka, H.; Saijo, K.; Takenaka, M.; Hashimoto, T. *Macromolecules* **2007**, *40*, 5923–5933.
(30) Mita, K.; Tanaka, H.; Saijo, K.; Takenaka, M.; Hashimoto, T. *Polymer* **2008**, *49*, 5146–5157.
(31) Mita, K.; Takenaka, M.; Hasegawa, H.; Hashimoto, T. *Macromolecules* **2008**, *41*, 8789–8799.
(32) Mita, K.; Tanaka, H.; Saijo, K.; Takenaka, M.; Hashimoto, T. *Macromolecules* **2008**, *41*, 6780–6786.
(33) Mita, K.; Tanaka, H.; Saijo, K.; Takenaka, M.; Hashimoto, T. *Macromolecules* **2008**, *41*, 6787–6792.
(34) Seki, T.; Nagano, S. *Chem. Lett.* **2008**, *37*, 484–489.
(35) Kadota, S.; Aoki, K.; Nagano, S.; Seki, T. *J. Am. Chem. Soc.* **2005**, *127*, 8266–8267.
(36) Morikawa, Y.; Nagano, S.; Watanabe, K.; Kamata, K.; Iyoda, T.; Seki, T. *Adv. Mater.* **2006**, *18*, 883–886.
(37) Yu, H.; Iyoda, T.; Ikeda, T. *J. Am. Chem. Soc.* **2006**, *128*, 11010–11011.
(38) Becker, H. D. *Chem. Rev.* **1993**, *93*, 145–172.
(39) Inoue, K.; Komatsu, S.; Trinh, X.-A.; Norisuye, T.; Tran-Cong-Miyata, Q. *J. Polym. Sci., Part B: Polym. Phys.* **2005**, *43*, 2898–2913.
(40) Trinh, X.-A.; Fukuda, J.; Adachi, Y.; Nakanishi, H.; Norisuye, T.; Tran-Cong-Miyata, Q. *Macromolecules* **2007**, *40*, 5566–5574.
(41) Russell, T. P.; Hjelm, R. P., Jr.; Seeger, P. A. *Macromolecules* **1990**, *23*, 890–893.
(42) Wang, J.-Y.; Chen, W.; Russell, T. P. *Macromolecules* **2008**, *41*, 4904–4907.
(43) Ahn, H.; Ryu, D. Y.; Kim, Y.; Kwon, K. W.; Lee, J.; Cho, J. *Macromolecules* **2009**, *42*, 7897–7902.
(44) Stühn, B. *J. Polym. Sci., Part B: Polym. Phys.* **1992**, *30*, 1013–1019.
(45) Stühn, B.; et al. *Europhys. Lett.* **1992**, *18*, 427.
(46) Zhao, Y.; Sivaniah, E.; Hashimoto, T. *Macromolecules* **2008**, *41*, 9948–9951.
(47) Ryu, D. Y.; Shin, C.; Cho, J.; Lee, D. H.; Kim, J. K.; Lavery, K. A.; Russell, T. P. *Macromolecules* **2007**, *40*, 7644–7655.
(48) Leibler, L. *Macromolecules* **1980**, *13*, 1602–1617.
(49) Rosedale, J. H.; Bates, F. S.; Almdal, K.; Mortensen, K.; Wignall, G. D. *Macromolecules* **1995**, *28*, 1429–1443.

(50) Sakamoto, N.; Hashimoto, T. *Macromolecules* **1995**, *28*, 6825–6834.
(51) Benoit, H.; Wu, W.; Benmouna, M.; Mozer, B.; Bauer, B.; Lapp, A. *Macromolecules* **1985**, *18*, 986–993.
(52) Schulz, G. V. *Z. Phys. Chem.* **1939**, *B43*, 25–46.
(53) Zimm, B. H. *J. Chem. Phys.* **1948**, *16*, 1099–1116.
(54) Cochran, E. W.; Morse, D. C.; Bates, F. S. *Macromolecules* **2003**, *36*, 782–792.
(55) Russell, T. P. *Macromolecules* **1993**, *26*, 5819–5819.
(56) Callaghan, T. A.; Paul, D. R. *Macromolecules* **1993**, *26*, 2439–2450.
(57) Hargreaves, J. S.; Webber, S. E. *Macromolecules* **1984**, *17*, 235–240.
(58) Sinigersky, V.; Müllen, K.; Klapper, M.; Schopov, I. *Adv. Mater.* **2000**, *12*, 1058–1060.
(59) Jones, R. N. *Chem. Rev.* **1947**, *41*, 353–371.
(60) Chen, W.; Wang, J.-Y.; Wei, X.; Xu, J.; Balazs, A. C.; Matyjaszewski, K.; Russell, T. P. *Macromolecules* **2011**, *44*, 278–285.
(61) Chen, W.; Wei, X.; Balazs, A. C.; Matyjaszewski, K.; Russell, T. P. *Macromolecules* **2011**, *44*, 1125–1131.
(62) Kline, S. R. *J. Appl. Crystallogr.* **2006**, *39*, 895–900.
(63) Bates, F. S.; Hartney, M. A. *Macromolecules* **1985**, *18*, 2478–2486.
(64) Benoit, H.; Hadziioannou, G. *Macromolecules* **1988**, *21*, 1449–1464.
(65) Hashimoto, T.; Koizumi, S.; Hasegawa, H. *Macromolecules* **1994**, *27*, 1562–1570.
(66) Bidkar, U. R.; Sanchez, I. C. *Macromolecules* **1995**, *28*, 3963–3972.
(67) Sakurai, S.; Nomura, S. *Polymer* **1997**, *38*, 4103–4112.
(68) Fredrickson, G., H.; Helfand, E. *J. Chem. Phys.* **1987**, *87*, 697–705.
(69) Bates, F. S.; Rosedale, J. H.; Fredrickson, G. H.; Glinka, C. J. *Phys. Rev. Lett.* **1988**, *61*, 2229–2232.
(70) Bates, F., S.; Rosedale, J. H.; Fredrickson, G. H. *J. Chem. Phys.* **1990**, *92*, 6255–6270.